Available online at www.sciencedirect.com
ScienceDirect
Journal of Magnetic Resonance 189 (2007) 228–240
JMR Journal of Magnetic Resonance
www.elsevier.com/locate/jmr

Measurement of hyperpolarized gas diffusion at very short time scales

Michael Carl [a], G. Wilson Miller [b,*], John P. Mugler III [b,c], Scott Rohrbaugh [a], William A. Tobias [a], Gordon D. Cates Jr. [a,b]

[a] Department of Physics, University of Virginia, Charlottesville, VA, USA
[b] Center for In-Vivo Hyperpolarized Gas MR Imaging, Department of Radiology, University of Virginia, Charlottesville, VA, USA
[c] Department of Biomedical Engineering, University of Virginia, Charlottesville, VA, USA

Received 31 March 2007; revised 12 September 2007
Available online 15 September 2007

Abstract

We present a new pulse sequence for measuring very-short-time-scale restricted diffusion of hyperpolarized noble gases. The pulse sequence is based on concatenating a large number of bipolar diffusion-sensitizing gradients to increase the diffusion attenuation of the MR signal while maintaining a fundamentally short diffusion time. However, it differs in several respects from existing methods that use oscillating diffusion gradients for this purpose. First, a wait time is inserted between neighboring pairs of gradient pulses; second, consecutive pulse pairs may be applied along orthogonal axes; and finally, the diffusion-attenuated signal is not simply read out at the end of the gradient train but is periodically sampled during the wait times between neighboring pulse pairs. The first two features minimize systematic differences between the measured (apparent) diffusion coefficient and the actual time-dependent diffusivity, while the third feature optimizes the use of the available MR signal to improve the precision of the diffusivity measurement in the face of noise. The benefits of this technique are demonstrated using theoretical calculations, Monte-Carlo simulations of gas diffusion in simple geometries, and experimental phantom measurements in a glass sphere containing hyperpolarized ^{3}He gas. The advantages over the conventional single-bipolar approach were found to increase with decreasing diffusion time, and thus represent a significant step toward making accurate surface-to-volume measurements in the lung airspaces.

Keywords: Diffusion NMR; Hyperpolarized gas; Restricted diffusion; Surface-to-volume ratio; Pulse sequences; Lung MRI

1. Introduction

Magnetic resonance imaging of the hyperpolarized noble gases ^{129}Xe and ^{3}He is a powerful technique for studying aspects of lung structure and function not accessible with conventional ^{1}H MRI [1]. In particular, measurements of the apparent diffusion coefficient of inhaled ^{3}He have shown sensitivity to the enlargement of alveolar and acinar airspaces due to emphysema [2–8]. The primary attraction of diffusion-weighted MRI is that it allows one to probe length scales much smaller than an imaging voxel. For instance, conventional MRI of hyperpolarized gas has been successful in resolving length scales on the order of a millimeter, but this is still significantly larger than alveolar dimensions, which are on the order of 100 microns.

Diffusion-weighted NMR techniques use the diffusion of particles in a restricted system to obtain information about the surrounding microstructure. The length scale Δr probed by such techniques is related to the time t over which the diffusive motion is observed: $(\Delta r)^2 = 6Dt$, where D is the diffusion coefficient, or diffusivity, of the particles. In the case of free (unrestricted) diffusion, the diffusion coefficient is simply the self-diffusivity D_0 of the particles, while in a restricted environment the diffusion coefficient is smaller than D_0 and also becomes a function of the observation time: $D \to D(t)$.

For sufficiently short diffusion times, the time-dependent diffusivity $D(t)$ is related to the surface-to-volume ratio (S/V) of the space available for diffusion. Qualitatively, this

* Corresponding author. Fax: +1 434 924 9435.
E-mail address: Wilson.Miller@Virginia.edu (G. Wilson Miller).

1090-7807/$ - see front matter © 2007 Elsevier Inc. All rights reserved.
doi:10.1016/j.jmr.2007.09.006

characteristic can be understood by noting that at short time scales, only the particles nearest the walls exhibit reduced diffusivity [9]. Since the fraction of particles nearest the walls is proportional to the surface-to-volume ratio of the pore space, the ensemble average diffusivity is smaller than the free diffusivity D_0 by an amount proportional to S/V.

Mitra et al. have derived a quantitative relationship between the short-time behavior of the diffusion coefficient in a restricted environment and the surface-to-volume ratio of the surrounding structure [9]:

$$D(t) \approx D_0\left[1 - \alpha\frac{S}{V}\sqrt{D_0 t}\right], \quad \text{with} \quad \alpha \equiv \frac{4}{9\sqrt{\pi}}. \tag{1}$$

Thus for short diffusion times $D(t)$ varies linearly with $\sqrt{t}$, with a slope proportional to S/V, and approaches D_0 as t approaches zero. This result can be used to extract S/V from two or more measurements of D in the short-time-scale regime. This theoretical relationship has been validated using numerical simulations [10–12] and experimental NMR measurements of both water diffusion [13] and noble-gas diffusion [14,15] in various porous media.

Practical issues associated with measuring S/V in the lung air spaces using diffusion NMR of inhaled hyperpolarized gases have been discussed in recent publications [11,12]. The primary difficulties with such measurements arise from the fact that the time scales involved are much shorter than typically encountered in MR diffusion measurements. The short-time-scale regime suitable for S/V measurements is entered for $t < (V/S)^2/D_0$. The self-diffusivity of xenon dilute in air is approximately 0.14 cm^2/s at atmospheric pressure [16], while for helium the value is nearly 0.9 cm^2/s. Since the surface-to-volume ratio in the normal human lung is approximately 200 cm^{-1} [17], measurements of S/V in the lung using hyperpolarized ^{129}Xe would require diffusivity measurements at observation times less than 200 μs, while for ^3He the minimum necessary diffusion time is even smaller. Making precise and accurate diffusivity measurements at such short time scales is extremely challenging with existing diffusion-weighted NMR techniques [11,12,14,15].

The standard diffusion weighted sequence used in proton NMR is the pulsed-gradient spin-echo method introduced by Stejskal and Tanner [18]. Spin-echo-based techniques are often impractical for hyperpolarized-gas MRI, however, because large-flip-angle RF pulses must be handled carefully to avoid destroying the non-equilibrium longitudinal magnetization. At the short diffusion times necessary for S/V measurements in the lung, it may not be possible to execute a full 180° RF pulse between the diffusion-sensitizing gradient lobes anyway. Therefore we will consider gradient-echo-based pulse sequences here.

The conventional pulse sequence for measuring hyperpolarized-gas diffusion is shown in Fig. 1a. Following application of the excitation RF pulse, a bipolar pair of gradient pulses, each of width δ, is used to impart diffusion weighting to the MR signal. The diffusion time, henceforth referred to as Δ, is set by the time between the peaks of the two equal but opposite gradient pulses. In the Gaussian phase approximation, the magnitude S of the diffusion-attenuated MR signal is related to the signal magnitude S_0 in the absence of diffusion weighting by the expression

$$S = S_0 \exp[-bD(\Delta)], \tag{2}$$

where

$$b \equiv 4\pi^2 \int [k(t)]^2 \, dt, \quad \text{with} \quad k(t) \equiv \frac{\gamma}{2\pi}\int_0^t G(t')\, dt' \tag{3}$$

encapsulates the theoretical dependence of the MR signal on the diffusion-sensitizing gradient $G(t)$ [19]. By measuring the diffusion-attenuated MR signal for at least two different b values (e.g. $b_1 = 0$ and $b_2 > 0$), $D(\Delta)$ can be determined by fitting the measured values to Eq. (2). The diffusivity measured in this way is more correctly referred to as the *apparent* diffusion coefficient (D_{app}), since the measured value may also depend on the measurement parameters such as δ and b. Strictly speaking, the apparent diffusivity $D_{app}(\Delta)$ is equal to the true time-dependent diffusivity $D(\Delta)$ only for $\delta \ll \Delta$ (the so-called narrow pulse approximation) and in the limit of low b values [19,20]. Furthermore, it has been shown that the diffusing particles must not traverse a significant fraction of the pore space during each lobe of the diffusion-sensitizing gradient ($D_0\delta \ll 0.02a^2$, where a is the pore diameter) [21]. This requirement is inherently met inside the very-short-time regime suitable for S/V measurements (since $\delta \leqslant \Delta$), but the effects of violating this criterion would need to be considered for longer diffusion times.

The vast majority of hyperpolarized-gas diffusion measurements performed to date have been acquired using a diffusion time Δ on the order of a millisecond [2–8,14,15]. At this time scale, clinical gradient systems can easily generate diffusion-sensitizing gradients with large enough b values to yield cleanly measurable diffusion attenuations. At diffusion times approaching 100 μs, however, clinical gradient systems are unable to generate substantial diffusion attenuation using a single bipolar gradient. For instance, assuming a maximum gradient slew rate typical of clinical systems (200 mT/m/ms), the highest achievable b value for ^{129}Xe with $\Delta = 200$ μs is $b \approx 3 \times 10^{-4}$ s/cm^2, which results in a diffusion attenuation bD_0 less than 50 parts per million. Such a small difference is extremely difficult to measure cleanly in the face of typical noise levels and systematic errors.

In a recent paper [11], Conradi et al. examined the feasibility of hyperpolarized-gas diffusion NMR measurements of S/V in the lung and concluded that errors of only 10–20% result from operating at the edge of the very-short-time-scale regime and well outside the low-b-value limit, which are more experimentally friendly regimes. Although this is an encouraging result, it would still be difficult to make such measurements using conventional pulse-sequence techniques on clinical systems, even with these relaxed requirements. Thus the feasibility of

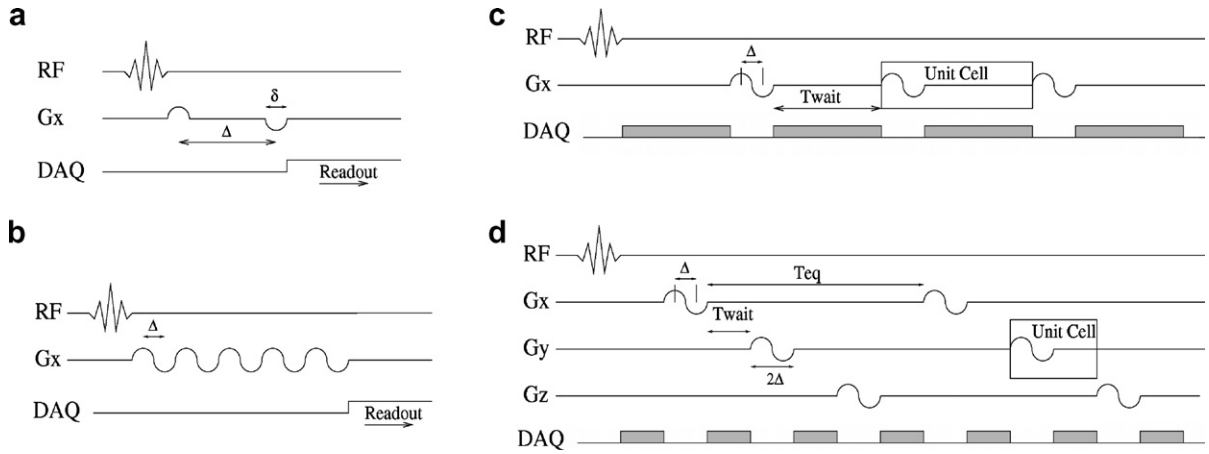

Fig. 1. (a) Conventional hyperpolarized noble-gas diffusion-weighted NMR pulse sequence utilizing a single pair of bipolar diffusion-sensitizing gradients. Explicitly shown are the diffusion time Δ and gradient duration δ. (b) Diffusion-weighted NMR pulse sequence utilizing an oscillating diffusion-sensitizing gradient waveform. The oscillating gradient effectively consists of N bipolar pulse pairs, each with the same value of Δ and b, concatenated with the intention that the total b value computes to Nb, while the fundamental diffusion time is simply Δ. (c) First proposed modification to the NMR pulse sequence utilizing an oscillating diffusion-sensitizing gradient, incorporating a time delay T_{wait} between consecutive bipolar gradients. (d) Further modification. Shown are six unit cells distributed along all three axes. Also shown is the diffusion time Δ, the wait time T_{wait}, and the resulting equilibration time $T_{\text{eq}} = 3\,T_{\text{wait}} + 2\,\Delta + 2\Delta$ between bipolar gradients along a given axis.

S/V measurements would be further enhanced by the development of improved methods for measuring short-time hyperpolarized gas diffusion.

The purpose of the present work is to address the fundamental experimental issue of how existing NMR diffusion techniques can be adapted to yield more accurate and precise diffusivity measurements at very short time scales. Our basic strategy is to concatenate a large number of bipolar diffusion-sensitizing gradients following each excitation RF pulse, to increase the diffusion attenuation of the MR signal while maintaining a fundamentally short diffusion time. This is the same strategy proposed by Gross and Kosfeld [22] and used by Schachter et al. [23] and Parsons et al. [24] to measure short-time water diffusion between closely packed beads using oscillating gradients. Our investigations show that even for narrow gradient pulses with low b values, however, the back-to-back concatenation of multiple bipolar gradients (to form an oscillating diffusion-sensitizing gradient, as in Fig. 1b), not only amplifies the diffusion attenuation of the MR signal, but also introduces systematic deviations of the measured diffusion coefficient from the true time-dependent diffusivity $D(t)$.

Since our ultimate goal is to obtain quantitatively accurate diffusivity measurements for extracting S/V, we introduce a new pulse sequence that incorporates several modifications to the oscillating-gradient approach. These changes are designed to minimize systematic differences between the resulting diffusivity measurement and the apparent diffusion coefficient that would be obtained by using the conventional single-bipolar pulse sequence shown in Fig. 1a. This distinction is important in the context of S/V measurements because modifications to the theoretical relationship between $D(t)$ and S/V given in Eq. (1) are available that apply to the apparent diffusion coefficient $D_{\text{app}}(\Delta)$, measured using the conventional single-bipolar technique [12,25]. We use theoretical calculations and Monte-Carlo simulations to optimize and validate this new pulse sequence, and finally use the refined technique to measure S/V in a simple structure and thereby experimentally demonstrate the SNR advantage of our strategy over the conventional single-bipolar method.

2. Pulse sequence design

The use of oscillating diffusion gradients to access shorter diffusion times was originally proposed by Gross and Kosfeld as a means to minimize the influence of restrictive barriers on the measured diffusion coefficient [22,19]. Oscillating gradients have also been used by Stepisnik and Callaghan to characterize the frequency spectrum of the diffusive motion [26,27]. These previous applications incorporated spin echoes, by placing 180° refocusing RF pulses between matched pairs of oscillating diffusion gradients, but their motivation for concatenating many bipolar diffusion gradients was the same as ours: to amplify the diffusion attenuation of the MR signal while maintaining a fundamentally short diffusion time.

In comparison, the present work focuses solely on time-domain diffusivity measurements without the use of spin echoes. Our goal is to make accurate diffusivity measurements at specific diffusion times, so that accurate S/V values can be extracted from the short-time behavior of the measured diffusion coefficient. The basic premise behind this approach is that by concatenating many bipolar diffusion-sensitizing gradients (as shown in Fig. 1b), the diffusion-attenuated MR signal becomes proportional to $\exp(-NbD)$ (confer Eq. (2)), where b represents the b-value of a single pair of bipolar gradient lobes (given by Eq. (3)) and N is the total number of such pairs. Although this approach works for free diffusion, in a restricted environ-

ment the resulting diffusion coefficient is not necessarily equal to the true particle diffusivity [19,20]. In fact, simulations presented in Section 3 show that even for very small *b*-values, back-to-back concatenation of individual bipolar gradients (Fig. 1b) does not yield the same apparent diffusion coefficient as the conventional single-bipolar arrangement (Fig. 1a). This deviation appears to be a consequence of the well-known edge enhancement effect [28], in which the spins nearest the walls of the structure are most restricted by their presence, resulting in lower de-phasing of these spins in the presence of a diffusion-sensitizing gradient and thus enhanced phase coherence near the edges. If the next bipolar diffusion gradient is applied while there is still such a systematic variation across the sample, all spins are not weighted equally for the next iteration and the diffusion attenuation does not compound simply as $\exp(-NbD)$.

To avoid this problem, we incorporate two modifications to the pulse sequence depicted in Fig. 1b. First, a wait time of duration T_{wait} is inserted after each bipolar pair of diffusion-sensitizing gradients to allow the uneven signal distribution to diffuse away before applying the next pair. A diagram of this arrangement is shown in Fig. 1c. In what follows, the bipolar gradient pulse pair plus the ensuing wait time will be referred to as a *unit cell*. The duration of each unit cell is given by $T_{\text{cell}} \equiv 2\Delta + T_{\text{wait}}$. Given the time limitation imposed by T_2^* decay, however, this wait time impairs the effectiveness of the overall strategy, which relies on imparting as much diffusion attenuation as possible.

To minimize the necessary wait time and thus maximize the number density of unit cells, the second modification we incorporate is to apply temporally consecutive bipolar diffusion gradients along orthogonal axes. Since the edge enhancement occurs along walls that are perpendicular to the direction of the magnetic-field gradient, this modification allows more time for the edge effect in the x direction to diffuse away, while imparting a diffusion weighting along the y and then z directions. Applying consecutive gradients along orthogonal axes will not completely decouple the resulting edge effects, as there will still be some cross-coherence that will either accumulate near sharp edges of a pore (''corner effect'') or be gently smeared out along smooth curves. However, this arrangement should dampen the rate at which the overall effects accumulate. The multi-axis version of our pulse sequence is shown in Fig. 1d. Note that with this arrangement, the effective wait time along each axis to allow the uneven signal coherence to equilibrate, which we will refer to as T_{eq}, is given by $3T_{\text{wait}} + 4\Delta$.

For porous structures without a macroscopic directional preference, the MR signal attenuation should be independent of the gradient axis used. In this case, the diffusivity measurement obtained using either the single-axis or the multi-axis implementation of our pulse sequence will represent the unique, isotropic diffusion coefficient of the medium. For non-isotropic pore structures, however, the single-axis implementation will yield a directionally dependent diffusivity measurement. The multi-axis implementation can also be applied to non-isotropic media, but the resulting diffusion coefficient will represent a directional average over the gradient axes used.

Note that the specific pulse sequences depicted in Fig. 1 are intended for global diffusion measurements, though regional measurements could be obtained following a selective preparation. Note also that although the maximum possible diffusion attenuation, subject to gradient slew-rate limitations, would be achieved using triangular or trapezoidal gradient shapes, in actual application it may be desirable to use sinusoidal gradient waveforms to minimize eddy current effects arising from large gradient magnitudes with fast switching times. The success of the pulse-sequence approaches described here, and the minimum wait times required for generating quantitatively accurate diffusivity measurements, are investigated in Section 3 using Monte-Carlo simulations of diffusion in restricted geometries.

2.1. Data sampling and analysis

In conventional diffusion-weighted MR pulse sequences, the diffusion-attenuated MR signal is not read out until all the diffusion gradients are complete. When using a long train of diffusion gradients following each excitation RF pulse, however, the gain in diffusion attenuation obtained by waiting to read-out the signal after the last unit cell would be partially offset by the fact that the available signal and therefore the SNR drops due to T_2^* decay during this time. Since our pulse sequence incorporates wait times between individual gradient pulse pairs, another feature of our method is that the diffusion-attenuated signal can be sampled during these wait times, rather than reading out only at end of the gradient train. This strategy allows the diffusion attenuation to be compounded as much as desired, without concern for the tradeoff between T_2^* decay and diffusion attenuation mentioned above, and also leads to a different analysis method than used for conventional techniques.

The signal $S_1(n)$ at the end of the nth unit cell corresponds to:

$$S_1(n) = A_1 \exp\left(-nbD - \frac{nT_{\text{cell}}}{T_2^*}\right), \tag{4}$$

where b is the conventionally defined value for a single bipolar gradient pair Eq. (3) and $n = 0, 1, \ldots, N$ starts at 0 since the signal is also sampled before the first unit cell. Signal dependencies that do not vary with n, such as amplifier gain and flip-angle effects, are carried by the coefficient A_1. To extract D from this relationship, the T_2^* contribution must be accounted for. This can be accomplished in a separate acquisition by sampling the free-induction-decay (FID) signal $S_2(n)$ during the same time intervals in the absence of any diffusion gradients:

$$S_2(n) = A_2 \exp\left(\frac{-nT_{\text{cell}}}{T_2^*}\right). \tag{5}$$

The same strategy for eliminating the T_2^* dependence has been used elsewhere [29] and resembles the $b = 0$ reference measurement typically used in the single-bipolar method. It follows that the ratio of these two signal measurements is given by:

$$R(n) \equiv \frac{S_1(n)}{S_2(n)} = \frac{A_1}{A_2}\exp(-nbD), \tag{6}$$

and a linear fit to $\ln[R(n)]$ vs. nb yields D. Note that the fraction A_1/A_2, which contains the effect of RF signal consumption between excitations, does not affect the calculation of D, and hence renders flip angle corrections unnecessary for our method.

The analysis method outlined above can be used for either the single-axis pulse sequence depicted in Fig. 1c or the multi-axis pulse sequence depicted in Fig. 1d. In the former case, one obtains a directionally dependent diffusivity, corresponding to the direction of the applied diffusion gradients, while in the latter case one obtains a directionally averaged diffusivity. If the same number of bipolar gradients are applied along each axis (that is, if N is a multiple of three), then the measured 3-D diffusivity will be the simple average of the directional diffusivities: $D_{\text{app}} = (D^x_{\text{app}} + D^y_{\text{app}} + D^z_{\text{app}})/3$. Such distinctions will be unimportant for isotropic diffusion, however.

2.2. Theoretical error calculation

The statistical error on the measurement of D using this method will of course depend on both the total number of unit cells N (and hence the total diffusion attenuation) and the individual statistical errors for each of the sampled data points $S_1(n)$ and $S_2(n)$. Since the individual errors are proportional to $1/\sqrt{T_{\text{wait}}}$, we anticipate a tradeoff between the increased SNR per data point resulting from lengthening T_{wait} and the increase in N made possible by shortening T_{wait}. This tradeoff can be analyzed quantitatively by considering the error on the slope of a linear fit $y = ax + b$ to a set of measured data points $(x_n,\ y_n)$:

$$\text{err}(a) = \sqrt{\frac{\sum_{n=0}^{N}\frac{1}{e_n^2}}{\sum_{n=0}^{N}\frac{x_n^2}{e_n^2}\sum_{n=0}^{N}\frac{1}{e_n^2} - \left(\sum_{n=0}^{N}\frac{x_n}{e_n^2}\right)^2}} \tag{7}$$

where e_n is the error on the measurement of y_n. For our purposes, $x_n = nb$ and $y_n = \ln[R(n)]$ so that $a = -D$. The functional form of e_n can be determined using standard error propagation formulas and is given by:

$$e_n = \frac{e_0}{\sqrt{T_{\text{wait}}}}\exp\left(\frac{nT_{\text{cell}}}{T_2^*}\right)\sqrt{1+\exp(2nbD)} \tag{8}$$

where e_0^2 is the mean-squared statistical noise per unit time.

These expressions can be substituted into Eq. (7) to generate a formula for the error on the measurement of D as a function of T_{wait}. Although there is not an exact closed-form solution for the value of T_{wait} that minimizes the error, the general features of this dependence are revealed by plotting the error versus T_{wait} for different values of Δ. Alternatively, one can obtain a simplified closed-form expression for the error by using an approximate form for e_n. Under the assumption that $e_n \approx e_0/\sqrt{T_{\text{wait}}}$ and hence is independent of n, evaluating Eq. (7) reveals that the minimum error occurs for $T_{\text{wait}} = \Delta$.

In Fig. 2, the exact form for the error has been evaluated numerically for several different diffusion times and is plotted as a function of the dimensionless ratio T_{wait}/Δ. The plot shows that for each value of Δ, the error on $D(\Delta)$ is minimized by choosing $T_{\text{wait}} \approx \Delta$, consistent with our simplified closed form solution. The dependence of the error on T_{wait} is rather flat around its minimum, however, so that not much would be lost by making T_{wait} a little higher than Δ, as will prove necessary to minimize edge-enhancement effects. It should be noted that the preceding theoretical analysis is independent of the requirement that the wait time be long enough that the diffusion attenuation compounds as $\exp(-nbD)$.

Although our multiple-bipolar pulse sequence will certainly yield larger diffusion attenuation than the conventional single-bipolar method, it does not necessarily follow that the apparent diffusion coefficient will be measured more precisely. To determine the advantage gained by using a large number of unit cells, we can compare the minimum error obtained from Eq. (7) with the error resulting from a conventional measurement using a single bipolar diffusion-sensitizing gradient. To make a fair comparison, we assume that for both methods the diffusion-attenuated signal is measured out to the same extent in time, denoted by T_{total}. Thus for the conventional method, T_{total} represents the signal integration time following the

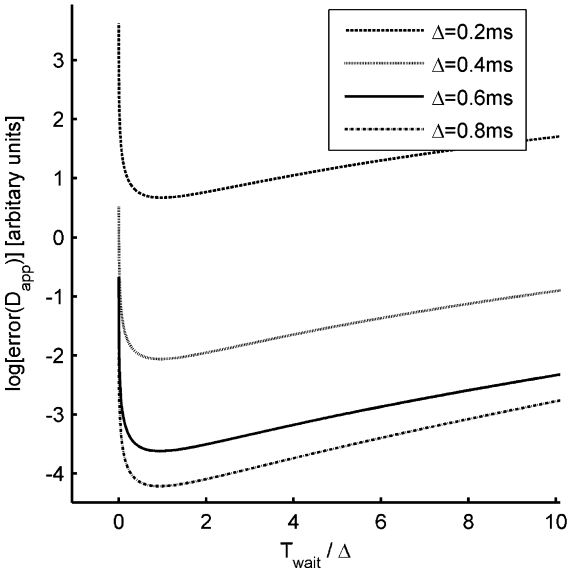

Fig. 2. Dependence of the statistical error in determining $D_{\text{app}}(\Delta)$ Eq. (7) on T_{wait}, plotted as a function of T_{wait}/Δ for several different values of Δ. Note that all the minima occur near $T_{\text{wait}} = \Delta$. We would like to emphasize that this result is independent of the specific characteristics of the porous structure being studied.

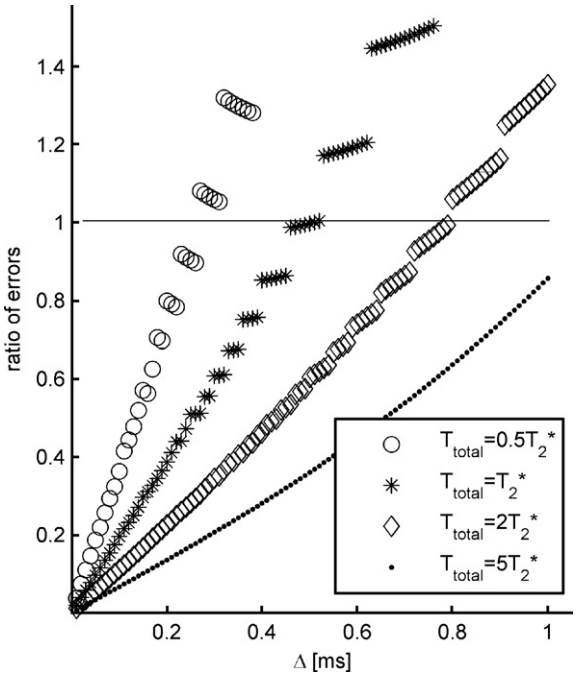

Fig. 3. Ratio of the statistical error on the measurement of D_{app} using our multiple-bipolar method Eq. (7) to the error using the conventional method Eq. (9), plotted as a function of Δ for different total readout times T_{total}. Our method yields greater precision for the combinations of Δ and T_{total} that have error ratios less than 1, and the noise advantage increases with decreasing Δ.

bipolar diffusion-sensitizing gradient, while for the multiple-bipolar method $T_{total} = NT_{cell}$. For the conventional pulse sequence, the statistical error on the measured diffusivity can also be determined using standard error propagation formulas:

$$\mathrm{err}(D) = e_0 \frac{\sqrt{T_{total}}}{T_2^*} \frac{1}{1 - \exp\left(\frac{T_{total}}{T_2^*}\right)} \sqrt{1 + \exp(2bD)} \qquad (9)$$

Fig. 3 shows the ratio of the error obtained using our multiple-bipolar method Eq. (7), with $T_{wait} = \Delta$, to the error obtained using the conventional method Eq. (9). The error ratio is plotted as a function of Δ for several different values of T_{total}. The discontinuities in the curves for each value of T_{total} result from the discrete jumps in the number of unit cells that can be fit within the fixed sampling time as Δ is varied. Our multiple-bipolar method yields greater precision for all combinations of Δ and T_{total} that have error ratios less than one. The plot shows that the advantage of our technique is strongest for smaller Δ.

3. Simulations

To test our pulse-sequence strategy for measuring very-short-time-scale diffusion and to determine appropriate values of T_{wait}, we performed Monte–Carlo simulations of gas diffusion in a restricted environment. The free diffusivity D_0 was chosen to be 0.14 cm^2/s, which is equivalent to xenon dilute in air at 1 atm [16]. All simulations were written in MATLAB (The MathWorks, Natick, MA) and performed on an ordinary desktop PC.

For each simulated run, a large number of diffusing particles ($10^5 \sim 10^7$) were initially distributed randomly within a sphere or cube of width 200–300 μm, which approximates alveolar dimensions. (The surface-to-volume ratio inside a 300-μm cube is 200 cm^{-1}, which is approximately the same as adult human lung [17]). At each time step δt, which represents the time between collisions, each particle was displaced a distance $\delta R = \sqrt{6D_0\delta t}$ in a random, isotropically chosen 3-D direction. If a move would penetrate a wall, the particle was reflected back into the structure about a line perpendicular to the wall. To reduce the total computation time while minimizing discretization errors, the time step δt was chosen to be larger than the mean scattering time for gas particles at standard temperature and pressure, while still small enough that the maximum diffusion step δR was at least two orders of magnitude smaller than the surrounding structure. Even with this shortcut, the total computation time was typically many hours per run.

In addition to tracking the Brownian motion, the simulation also included the ability to track the phase accumulated by each particle under the influence of time-varying diffusion gradients. All phases were initially set to zero, and the phase of each particle was advanced at each time step according to the magnetic field at its current location. At any given time step, the magnitude of the vector sum of all particle phases could be calculated to yield the MR signal, which could then be used to calculate the apparent diffusion coefficient measured using the simulated diffusion gradients. By computing the ensemble average displacement the true time-dependent diffusivity $D(t)$, which is not dependent on the NMR gradient method used, could also be calculated at each time step according to:

$$D(t) = \frac{\left\langle \left[\vec{r}_j(t) - \vec{r}_j(0)\right]^2 \right\rangle_j}{6t} \qquad (10)$$

This quantity will be referred to as the true diffusivity, or simply $D(t)$, to distinguish it from D_{app} as measured using diffusion-weighted MR techniques.

3.1. Investigating T_{wait}

In order to evaluate the minimum necessary wait time discussed earlier, we simulated MR measurements of restricted diffusion for two different pulse-sequence arrangements. To isolate the edge-enhancement contribution to the compounded signal attenuation from the effects of wide gradient pulses, we first simulated the application of 10 consecutive bipolar pairs of narrow ($\delta = 0$) diffusion-sensitizing gradient pulses, all oriented along the same axis (hence T_{eq} was equal to T_{wait}). These simulations were performed in a 200 μm sphere at diffusion times ranging from $\Delta = 50$ μs to 500 μs. Low b-values were used, such that $bD_0 \approx 0.01$ for each bipolar gradient. For a given value of Δ separating the two gradient pulses in each pair,

the equilibration time T_{eq} between pairs was varied from 0 to 10Δ. The diffusion-attenuated signal was computed at the end of the gradient pulse train and set equal to $\exp(-10bD_{app})$ to extract a measurement of $D_{app}(\Delta)$.

Fig. 4a shows the dependence of the measured apparent diffusion coefficient on T_{eq} for five different values of Δ ranging from 50 to 500 μs. The horizontal lines represent the respective values of $D_{app}(\Delta)$ that would be measured using the conventional single-bipolar method, which in this case ($\delta = 0$) is the same as the true diffusivity $D(t)$. For every Δ, the measured diffusivity is artificially low for $T_{eq} = 0$. One can see from the example of $\Delta = 0.05$ ms, that for $T_{eq} = 0$, the measured diffusivity starts at the correct value of $D(t)$ for 0.5 ms ($=10\Delta$). This can easily be understood by the fact that for narrow pulses and zero wait time, the second diffusion gradient of any unit cell effectively cancels the first diffusion gradient of the next unit cell, so that one winds up with the exact sequence to measure $D(t = 10\Delta)$. As the wait time is increased from zero, the measured diffusion coefficient asymptotically approaches the true diffusivity $D(t)$ for the given Δ, although the rate of approach varies with Δ. Closer inspection reveals that equilibration time T_{eq} required to reach a given level of accuracy scales with $\sqrt{\Delta}$. This means that smaller values of Δ require a proportionately longer wait time to reach the same level of accuracy, but the absolute wait time still decreases with decreasing Δ.

In the second set of simulations, we examined the systematic deviation of D_{app}, as measured using our multiple-bipolar pulse sequence, from that measured using the conventional single-bipolar pulse sequence, using sinusoidal diffusion gradients with $\delta = \Delta = 100$ μs. The sinusoidal gradient was constructed assuming a maximum slew rate of 200 mT/m/ms, resulting in a very low b value such that $bD_0 \ll 1$ for each bipolar gradient. Two different arrangements of the diffusion-sensitizing gradients were considered. For the data points labeled as 1-D, all diffusion-sensitizing gradients were applied along the same coordinate axis as depicted in Fig. 1c, while for the points labeled 3-D, the applied gradients were rotated among the three principal axes as depicted in Fig. 1d.

Fig. 4b shows the signal ratio $R(n)$ (given by Eq. (6)) sampled during the wait times between each bipolar gradient pair, for several values of T_{wait} ranging from 0 to 4Δ. All curves coincide for the first two data points, since the pulse sequences are identical up to the first unit cell. For zero wait time (triangular markers), subsequent unit cells do not produce the same diffusion attenuation as the first cell. This effect causes the measured value of D_{app}, obtained by fitting the simulated data points to Eq. (6), to be lower than would be obtained if only the first two data points were used. The elbow at the second data point straightens out as the wait time is increased, and the measured value of D_{app} approaches the value obtained using a single bipolar pair as shown previously in Fig. 4a. As expected, the curve for $T_{wait}(3\text{-D}) = 0$ is the same as that for T_{wait} (1-D) $= 4\Delta$. This result confirms our expectation that applying consecutive bipolar gradient pairs along orthogonal axes decouples the effects of neighboring pairs, and yields an effective wait time given by T_{eq}. Note that for T_{wait} (3-D) $= 2\Delta$, which corresponds to the pulse sequence depicted in Fig. 1d, the desired asymptote (solid line) has been reached.

Finally, to directly explore the edge effect responsible for the behavior discussed in the previous paragraphs, we simulated short-time-scale MR diffusion measurements inside a 300-μm cube. Fig. 5a shows the simulated 1-D projection of the signal coherence between parallel sides following

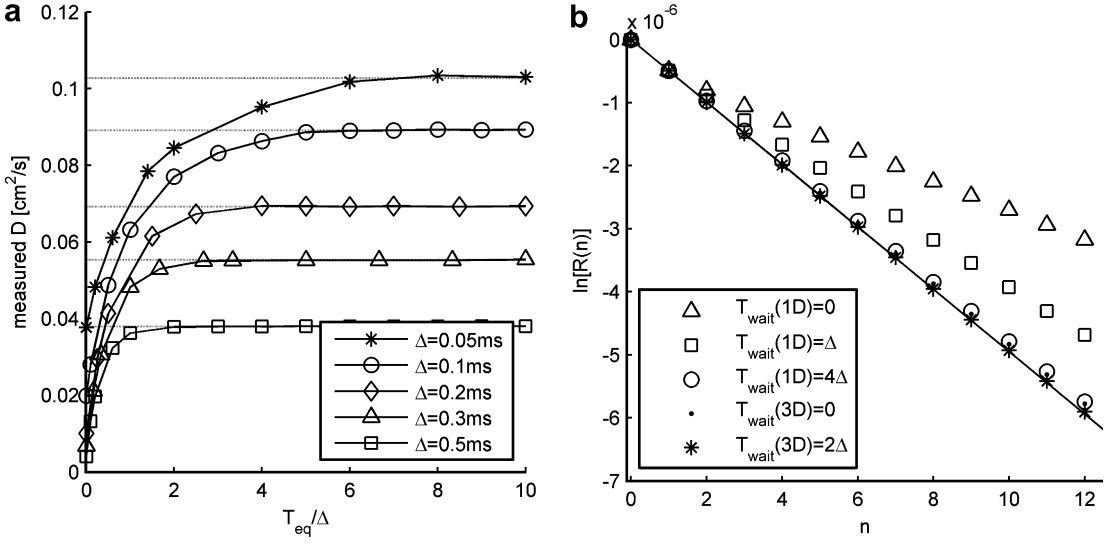

Fig. 4. (a) Simulated results showing the asymptotic approach of the apparent diffusivity, measured in a 200-μm sphere using 10 pairs of narrow gradient pulses, to the value measured using a single pair of diffusion-sensitizing gradients (dotted lines), as the equilibration time T_{eq} is varied from 0 to 10Δ for several diffusion times Δ. (b) Simulated measurements showing the underlying deviation of the diffusion-weighted signal from a pure exponential, using our multiple-bipolar method inside a 200 μm sphere with $\Delta = 100$ μs. Plotted is $\ln[R(n)]$ Eq. (6) for several wait times ranging from 0 to 4Δ, for both 1-D and 3-D gradient trains.

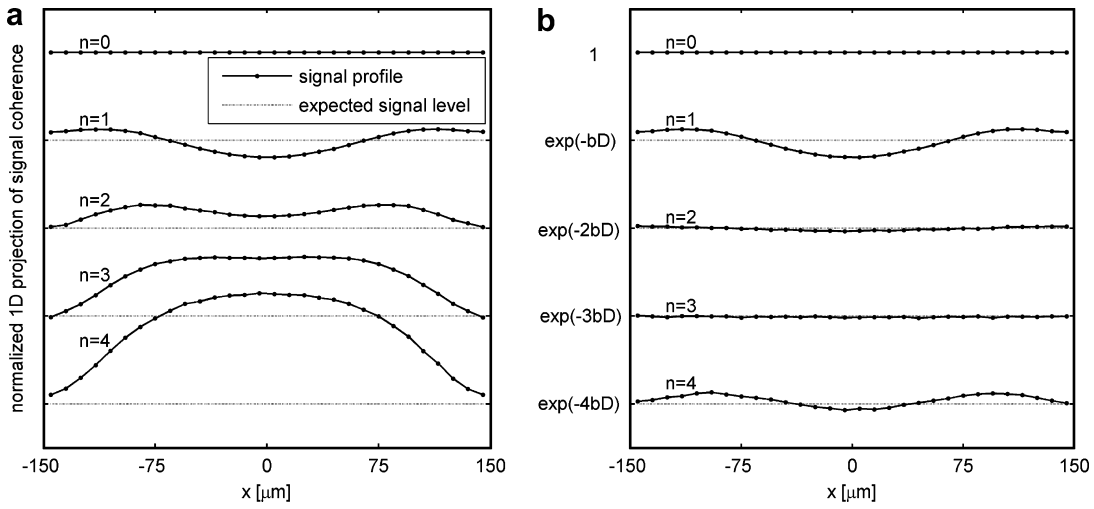

Fig. 5. (a) Simulated 1-D projections of the signal coherence between parallel sides of a 300-μm cube, following each of four bipolar diffusion-sensitizing gradients, all applied along the same directional axis with no wait time between them (per the pulse sequence in Fig. 1b). For comparison the expected signal levels (dashed lines), corresponding to $\exp(-nbD_{app})$, are also shown. (b) A similar plot of the 1-D signal coherence using the multi-axis sequence shown in Fig. 1d with $T_{wait} = \Delta$. Note that in this case the average signal declines as $\exp(-nbD_{app})$, which is the desired behavior.

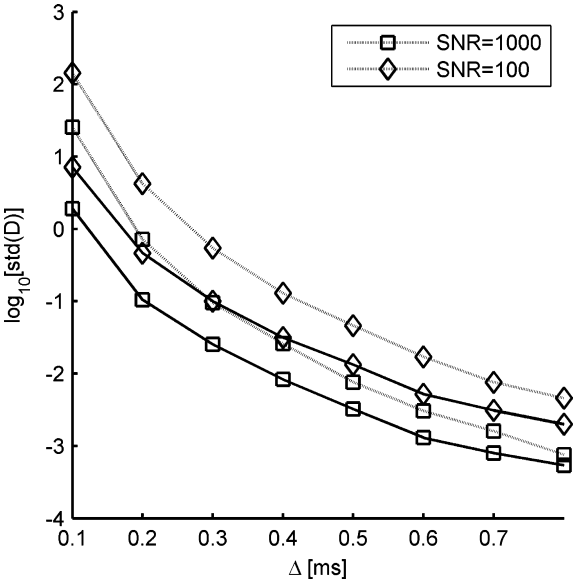

Fig. 6. Standard deviation in simulated measurements of $D_{app}(\Delta)$, plotted as a function of Δ, using both our multi-axis pulse sequence (black lines) as well as the conventional method (gray lines). Observe that for $\Delta < 0.3$ ms, our sequence with SNR = 100 produces less statistical error than the standard technique with SNR = 1000.

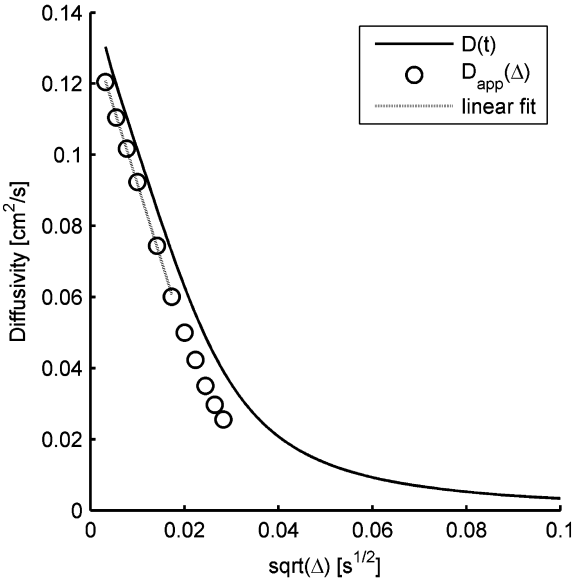

Fig. 7. Simulated values for $D(t)$ and $D_{app}(\Delta)$ inside a 200-μm cube, the latter measured using the 3-D version of our multiple-bipolar pulse sequence, displayed as a function of $\sqrt{\Delta}$ together with the linear fit that yields S/V. The measured values are systematically low, which necessitates the use of the modified value α_{sine} to extract accurate S/V from the MR diffusion measurements.

each cycle of a sinusoidally varying magnetic-field gradient, which corresponds to the pulse sequence depicted in Fig. 1b. Also shown are the expected signal levels $\exp(-nbD_{app})$ with $n = 1, 2, 3, 4$. Note the signal enhancement at the edges of the box immediately following application of the first bipolar gradient ($n = 1$), and that the average signal agrees with $\exp(-bD_{app})$ at this point. The signal profile for $n = 1$ conforms to our conventional notion of the edge effect, resembling Fig. 7 of Ref. [28]. For $n > 1$, however, the enhanced signal does not simply build up along the edges, but also begins to diffuse toward the center. Upon repeated application of the bipolar diffusion gradient, the simulation shows that the signal profile eventually becomes higher at the center of the box than at the edges. Furthermore, for $n > 1$ the average signal is systematically higher than $\exp(-nbD_{app})$, in agreement with Fig. 4.

By contrast, Fig. 5b shows the evolution of the signal profile for the 3-D pulse sequence depicted in Fig. 1d. After the first bipolar gradient ($n = 1$), the signal profile is the same as in the 1-D case. In the 3-D case, however,

the next bipolar gradient ($n = 2$) is applied along an orthogonal direction, and thus the signal profile along the axis shown here appears unaffected by this gradient. In fact, by the end of the second gradient the uneven signal distribution along the direction of the first gradient has almost entirely diffused away, and it appears to be completely resolved at $n = 3$. Thus the next bipolar gradient ($n = 4$), which is applied along the same direction as the first, does indeed produce nearly the same signal profile as $n = 1$. Note also that unlike the 1-D case, the average signal decreases proportional to $\exp(-nbD_{app})$, which is the desired behavior.

3.2. Noise comparison

To establish whether our new method actually does provide a more precise measure of the diffusion coefficient at the very-short time scales relevant to S/V measurements in the lung, we simulated diffusivity measurements inside a 200-μm sphere using both the conventional single-bipolar method and our modified multiple-bipolar pulse sequence at diffusion times ranging from 100 to 800 μs. To simulate the effects of measurement noise, Gaussian white noise was added to each of the simulated signal magnitudes before computing the measured diffusion coefficient. Two different noise levels were simulated, corresponding to SNR of 100 and 1000. The simulation was repeated 100 times for each Δ and each SNR level, and the standard deviation was calculated for each group of 100 measurements.

In Fig. 6, the standard deviations of the simulated diffusivity measurements are plotted as a function of Δ for both the conventional single-bipolar method (gray lines) and our multiple-bipolar method (black lines). Note that our method provides better precision at all diffusion times shown, and that the advantage increases for smaller values of Δ. This behavior is consistent with the results of the theoretical error calculations shown in Fig. 3. For the smallest diffusion time considered (100 μs), our new pulse sequence provides almost an order of magnitude better precision than the conventional method.

3.3. S/V measurements

To extract accurate S/V measurements from short-time MR diffusion measurements using realistic gradients, the effects of wide gradient pulses must be accounted for. Zielinski and Sen explored this issue analytically [25], and found that for gradient pulses with a square profile and $\delta = \Delta$ (in maximal violation of the narrow-pulse criterion), the time-dependent diffusivity curve still approaches D_0 linearly as $\sqrt{\Delta}$ goes to zero (confer Eq. (1)), but with a steeper slope than for narrow gradient pulses, and that accurate S/V values can be obtained from this slope if the correct proportionality constant α is used. This result was confirmed by Miller et al. in a recent study of simulated 2-D diffusion [12], in which the appropriate proportionality constants α_{sine} and $\alpha_{triangle}$ for sinusoidal and triangular pulse shapes were also determined.[1]

To validate the Miller results for wide gradient pulses in the case of 3-D diffusion, MR diffusion measurements using a single bipolar gradient were simulated inside a 200-μm cube using four different pulse shapes: narrow, triangular, sinusoidal, and square. We found that the correct relationship between S/V and the initial slope of the diffusivity curve occurs at $\alpha = 0.253$ for narrow pulses, $\alpha_{triangle} = 0.297$ for triangular pulse shapes, $\alpha_{sine} = 0.298$ for sinusoidal pulses and finally $\alpha_{square.} = 0.317$ for square pulses. Our results for narrow pulses and square pulses are within 1% of the Mitra ($\alpha = 0.251$) and Zielinski ($\alpha_{square} = 0.314$) analytic results, and within 2% and 1% of the Miller simulation results for sinusoidal and triangular gradients, respectively, after extrapolating them from 2-D to 3-D ($\alpha_{sine} = 0.291$ and $\alpha_{triangle} = 0.300$).

Finally, we simulated the multi-axis version of our new pulse sequence (Fig. 1d) in the same 200-μm cube in the attempt to measure $D_{app}(\Delta)$ and subsequently S/V. Fig. 7 shows several measured diffusion coefficients, displayed as a function of $\sqrt{\Delta}$, together with the true diffusivity curve $D(t)$ obtained directly from the simulated particle motion Eq. (10). Applying the value for α_{sine} obtained above to the fit slope of the short-time asymptote, we found the simulated diffusion measurement of S/V to be 293 cm^{-1}, in good agreement with the expected value of 300 cm^{-1}.

4. Experiments

To demonstrate the use of our pulse sequence to make quantitative experimental diffusion measurements at time scales relevant to S/V in the lung, we measured time-dependent gas diffusion inside a sphere of approximately one-inch diameter. The sealed pyrex cell contained 2.7 atm ^{3}He along with ~0.1 atm nitrogen and a small quantity of rubidium. Prior to each NMR measurement, the cell was optically pumped for ~18 h by circularly polarized diode laser light and then transported approximately one mile from the polarization apparatus to the scanner inside a homemade, battery-powered solenoid electromagnet.

The pulse sequence depicted in Fig. 1d was implemented on a commercial whole-body scanner (Siemens Sonata) and used to measure the diffusivity of the ^{3}He gas at diffusion times ranging from 200 μs to 3800 μs. A measurement of the surface-to-volume ratio inside the sphere was extracted by fitting the resulting measurements to the generalized form of Eq. (1), using the value of α for sinusoidal pulses found in the previous section.

[1] To minimize confusion over notation, we would like to point out that the proportionality constant α referred to in the present work is defined slightly differently than in Ref. [12]. In that paper, the $1/d$ dimensional dependence was carried separately from α, whereas in the present work this dependence has been absorbed into the definition of α given by Eq. (1).

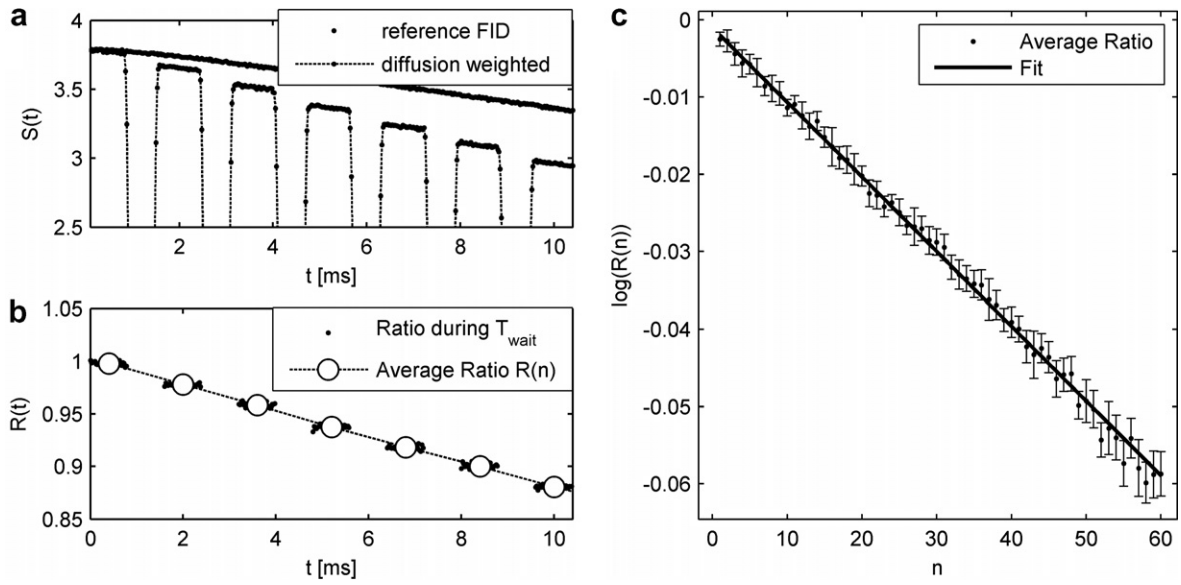

Fig. 8. (a) Experimentally measured MR signal magnitudes, from both the reference acquisition S_2 Eq. (5) and the diffusion-attenuated acquisition S_1 Eq. (4). (b) The signal ratio $R(t) \equiv S_1/S_2$ Eq. (6). Only the data sampled during T_{wait} are shown here, along with the average values (open circles) and exponential fit (dashed line) from which D_{app} is calculated. (c) Experimental data obtained with $\Delta = 200$ μs, along with the fit line that yields the measurement of D_{app}.

Representative experimental signal data is shown in Fig. 8a. Each data point represents the magnitude of the demodulated MR signal, integrated over a sampling time of 25 μs. The continuous curve is from the T_2*-decay reference acquisition, while the dotted curve shows the signal evolution during the diffusion-weighted acquisition. Fig. 8b shows the ratio $R(t)$ of corresponding data points during the wait times, with the average value superimposed (circles). The dotted line represents the exponential fit, which allows the calculation of D. Only six unit cells are displayed, to facilitate comparison with the sequence shown in Fig. 1d. Each such measurement was repeated 5 times using a flip angle of 15° and the results averaged to arrive at diffusivity measurements with associated error estimates.

Fig. 8c shows the mean values of the diffusion-attenuated ratio, sampled during each wait time, from the acquisition of $N = 60$ unit cells at $\Delta = 200$ μs (a single bipolar gradient is applied between the acquisition of each signal average shown here). This figure highlights the essence of our experimental technique: Whereas the difference between neighboring data points is too small to yield a reliable measurement of the diffusion attenuation (e.g., note that in some cases the next data point is higher than the previous one), the compounded diffusion attenuation from the accumulation of many such data points can be cleanly fit.

Fig. 9a shows all the experimentally measured diffusivities plotted versus $\sqrt{\Delta}$. From the fit slope, we obtain a surface-to-volume measurement of $224 \pm 4\ \text{m}^{-1}$. This result is within 5% of the nominal value of $236\ \text{m}^{-1}$ for a 1-inch sphere.

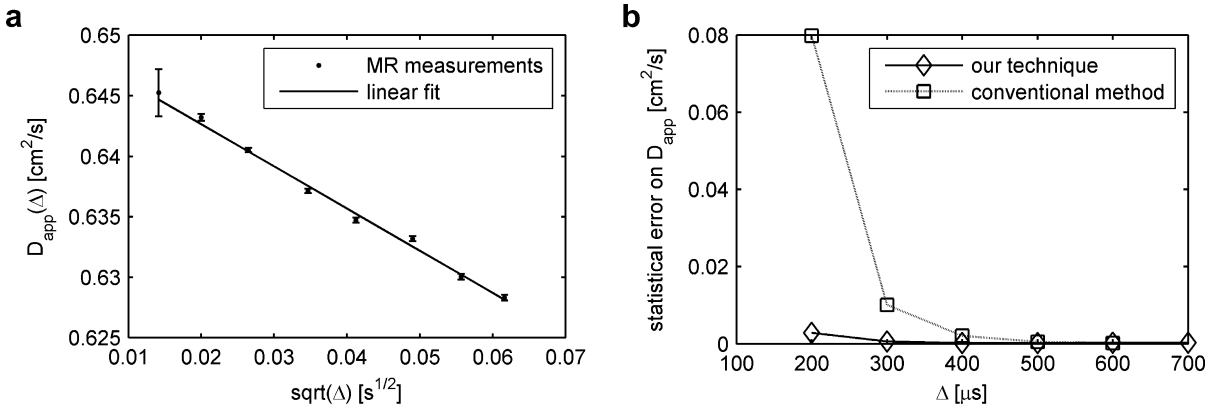

Fig. 9. (a) Experimentally measured values of $D_{\text{app}}(\Delta)$, plotted as a function of $\sqrt{\Delta}$ for a 1-inch sphere containing 2.7 atm of hyperpolarized ^{3}He, along with the linear fit that yields $S/V \approx 224\ \text{cm}^{-1}$. (b) Statistical error on $D_{app}(\Delta)$ as a function of Δ, from equivalent measurements using both our new technique and the conventional single-bipolar pulse sequence.

In order to verify the SNR advantage of our pulse sequence for measuring very-short-time diffusion over the conventional single-bipolar method, we also attempted to measure the diffusivity at diffusion times ranging from 200 to 700 μs using both techniques. To provide a fair comparison, the FID was sampled out to the same extent in both methods. As expected, we were not able to extract reliable diffusion coefficients at the shortest diffusion times (200–400 μs) using the conventional method. However, we were still able to track the statistical errors on these measurements. Fig. 9b shows the experimental statistical errors on D_{app} obtained at each Δ value using each of the two methods. In agreement with earlier theoretical and simulated results, the errors are of comparable size for larger values of Δ, while the error increases much more rapidly for smaller Δ using the conventional method.

5. Discussion

The time-dependent diffusion coefficient $D(t)$ appearing in Eq. (1), which can be used to determine S/V in the very-short-time-scale limit, represents the diffusivity averaged over all possible directions. Thus for non-isotropic pore spaces, the diffusion coefficient measured using our multi-axis pulse sequence (Fig. 1d) is more suitable than a single-axis implementation for extracting accurate S/V values. On the other hand, if the diffusion coefficient in a particular direction is desired, then the basic method described here could still be used but with all diffusion gradients applied along the same axis (Fig. 1c). However, maintaining the same equilibration time and thus the same level of systematic errors would require longer wait times than the multi-axis implementation. Therefore some of the noise advantage over the conventional single-bipolar technique would be lost, because fewer bipolar gradients could be applied within the limit of T_2^* signal decay. This general tradeoff between accuracy and precision is an inherent property of our method. Increasing the equilibrium time will suppress systematic errors arising from edge effects, but will also tend to diminish the statistical precision of the diffusivity measurement.

An important consideration for the practical application of our pulse sequence is how to select the particular value of T_{wait} to use. From the standpoint of statistical precision, Fig. 2 indicates that the optimum wait time is equal to Δ, but Fig. 4 shows that the wait time required to achieve a given level of accuracy may be larger than Δ, and furthermore the necessary normalized wait time T_{eq}/Δ increases as Δ decreases. Another important factor is that the wait time required for a given application should also depend on the characteristic length scale L of the pore space. Dimensional analysis suggests that the required wait time should scale with the quantity $L(\Delta/D_0)^{1/2}$, which has units of time. For surface-to-volume measurements, where L can be taken to be V/S, this means that one must already have an idea of what S/V is to design an appropriate pulse sequence for measuring it. For most applications this should not be a problem, however, since it is likely that S/V will be known to lie in a general range. Fig. 2 shows that from a standpoint of measurement precision, as long as T_{wait} is greater than Δ, the penalty for using a larger value of T_{wait} is not overwhelming. From the complementary standpoint of measurement accuracy, therefore, one should probably err on the side of choosing T_{wait} a little longer than necessary. Although the foregoing discussion provides a useful guide to the issues involved, further investigation is necessary to determine a more generally valid criterion for T_{wait}.

Although the experimental regime explored in the present work (^{3}He diffusion inside a pressurized 1-inch sphere) does not require our specialized pulse sequence to obtain MR diffusion measurements at short enough time scales for S/V quantification, it provides a test bed for comparing our technique with the conventional diffusion-weighted pulse sequence. Whereas the very-short-time regime suitable for S/V measurements extends out beyond 100 ms for this phantom, we purposefully challenged our technique by making measurements at diffusion times as low as $\Delta = 200$ μs, which is within the short-time regime for alveolar length scales as discussed above. Our method clearly outperformed the conventional single-bipolar method in this regime. In future work, we will test our technique in more challenging experimental situations, such as in more elaborate phantoms and in lung airspaces *in vivo*, having much higher surface-to-volume ratios and thus much shorter time-scale requirements. These studies will concentrate on experimental regimes in which other groups have observed the breakdown of other diffusion-weighted pulse sequences at atmospheric pressure [15,29]. Future efforts will also concentrate on adapting our basic strategy, which in its present form yields global diffusion measurements, to provide spatially resolved measurements by incorporating k-space readout into our pulse sequence.

Potentially serious obstacles to making accurate measurements in more challenging experimental regimes will be systematic errors caused by gradient infidelity. Possible sources include eddy currents, concomitant gradients, and background gradients due to magnetic-susceptibility mismatch at pore boundaries. Background gradients in particular have been previously observed to alter the measured diffusion coefficients in porous structures [30,31], though such effects can often be reduced by the use of spin echoes [32]. If we encounter similar problems, it may be possible to incorporate such strategies into our pulse sequence, for instance by increasing the wait time to allow refocusing RF pulses to be inserted between consecutive bipolar gradients. This would actually cause our pulse sequence to more closely resemble other pulse sequences that use oscillating gradients [22,26,27]. Such modifications would need to be implemented carefully, however, to avoid the general problems associated with the use of large-flip-angle RF pulses on hyperpolarized nuclei that were mentioned in the introduction.

6. Conclusion

We have demonstrated a new pulse-sequence strategy for measuring hyperpolarized-gas diffusion at very short time scales. This pulse sequence uses multiple pairs of bipolar diffusion-sensitizing gradient pulses to amplify the attenuation of the MR signal, which would otherwise be too small to yield robust diffusivity measurements. To prevent effects due to edge-enhancement of the MR signal from compounding along with the diffusion attenuation, consecutive gradient-pulse pairs are applied along orthogonal directions and separated by a brief wait time. For isotropic media, this strategy leads to apparent diffusion coefficients that are the same as would be measured using a single pair of bipolar gradient pulses, but with greatly enhanced precision in the face of measurement noise. For non-isotropic media, the resulting diffusivity measurement represents a directional average over the gradient axes used. At very short diffusion times, such measurements can be used to extract accurate measurements of the surface-to-volume ratio of the pore space, after correcting for the effects of wide gradient pulses.

The noise advantage of our technique over the conventional single-bipolar method has been demonstrated using theoretical calculations, numerical simulations, and experiments, and is found to increase for smaller diffusion times. This is due to the fact that within the time limitation imposed by T_2^*, one can apply more unit cells for smaller values of Δ and further amplify the diffusion attenuation. Fig. 9b shows that the difference in precision increases rapidly for diffusion times below 500 μs. In their paper on the feasibility of S/V measurements in the lung [11], Conradi et al. conclude that diffusion times less than 125 us are required to make reasonably accurate S/V measurements using helium diffusion, which extrapolates to approximately 500 μs for xenon diffusion. Taken together, these results bode well for the possibility of making accurate S/V measurements in the lung using our technique.

Acknowledgment

Research supported by Siemens Medical Solutions and by grant R01-HL079077 from the National Heart, Lung, and Blood Institute. The content is solely the responsibility of the authors and does not necessarily represent the official views of the National Heart, Lung, and Blood Institute or the National Institutes of Health.

References

[1] H.U. Kauczor, A. Hanke, E.J.R. van Beek, Assessment of lung ventilation by MR imaging: current status and future perspectives, Eur. Radiol. 12 (2002) 1962–1970.

[2] X.J. Chen, L.W. Hedlund, H.E. Möller, M.S. Chawla, R.R. Maronpot, G.A. Johnson, Detection of emphysema in rat lungs by using magnetic resonance measurements of ^{3}He diffusion, Proc. Natl. Acad. Sci. USA 97 (2000) 11478–11481.

[3] B.T. Saam, D.A. Yablonskiy, V.D. Kodibagkar, J.C. Leawoods, D.S. Gierada, J.D. Cooper, S.S. Lefrak, M.S. Conradi, MR imaging of diffusion of ^{3}He gas in healthy and diseased lungs, Magn. Reson. Med. 44 (2000) 174–179.

[4] M. Salerno, E.E. de Lange, T.A. Altes, J.D. Truwit, J.R. Brookeman, J.P. Mugler III, Emphysema: hyperpolarized helium-3 diffusion MR imaging of the lungs compared with spirometric indices—initial experience, Radiology 222 (2002) 252–260.

[5] A.J. Swift, J.M. Wild, S. Fichele, N. Woodhouse, S. Fleming, J. Waterhouse, R. Lawson, M.N.J. Paley, E.J.R. Van Beek, Emphysematous changes and normal variation in smokers and COPD patients using diffusion ^{3}He MRI, Eur. J. Radiol. 54 (2005) 352–358.

[6] S.B. Fain, S.R. Panth, M.D. Evans, A.L. Wentland, J.H. Holmes, F.R. Korosec, M.J. O'Brien, H. Fountaine, T.M. Grist, Early emphysematous changes in asymptomatic smokers: detection with ^{3}He MR imaging, Radiology 239 (2006) 875–883.

[7] J.F. Mata, T.A. Altes, J. Cai, K. Ruppert, W. Mitzner, K.D. Hagspiel, B. Patel, M. Salerno, J.R. Brookeman, E.E. de Lange, W.A. Tobias, H.T. Wang, G.D. Cates, J.P. Mugler III, Evaluation of emphysema severity and progression in a rabbit model: comparison of hyperpolarized ^{3}He and ^{129}Xe diffusion MRI with lung morphometry, J. Appl. Physiol. 102 (2007) 1273–1280.

[8] T.S.K. Tanoli, J.C. Woods, M.S. Conradi, K.T. Bae, D.S. Gierada, J.C. Hogg, J.D. Cooper, D.A. Yablonskiy, In vivo lung morphometry with hyperpolarized ^{3}He diffusion MRI in canines with induced emphysema: disease progression and comparison with computed tomography, J. Appl. Physiol. 102 (2007) 477–484.

[9] P.P. Mitra, P.N. Sen, L.M. Schwartz, P. Le Doussal, Diffusion propagator as a probe of the structure of porous media, Phys. Rev. Lett. 68 (1992) 3555–3558.

[10] P.P. Mitra, P.N. Sen, L.M. Schwarz, Short-time behavior of the diffusion coefficient as a geometrical probe of porous media, Phys. Rev. B 47 (1993) 8565–8574.

[11] M.S. Conradi, M.A. Bruns, A.L. Sukstanskii, S.S. Gross, J.C. Leawoods, Feasibility of diffusion-NMR surface-to-volume measurements tested by calculations and computer simulations, J. Magn. Reson. 169 (2004) 196–202.

[12] G.W. Miller, M. Carl, J.F. Mata, G.D. Cates, J.P. Mugler III, Simulations of short-time diffusivity in lung airspaces and implications for S/V measurements using hyperpolarized-gas MRI, IEEE Trans. Med. Imag., in press, doi:10.1109/TMI.2007.903192.

[13] L.L. Latour, K. Svoboda, P.P. Mitra, C.H. Sotak, Time-dependent diffusion of water in a biological model system, Proc. Natl. Acad. Sci. USA 91 (1994) 1229–1233.

[14] R.W. Mair, D.G. Cory, S. Peled, C.H. Tseung, S. Patz, R.L. Walsworth, Pulsed-field-gradient measurements of time-dependent gas diffusion, J. Magn. Reson. 135 (1998) 478–486.

[15] R.W. Mair, G.P. Wong, D. Hoffman, M.D. Hürlimann, S. Patz, L.M. Schwartz, R.L. Walsworth, Probing porous media with gas diffusion NMR, Phys. Rev. Lett. 83 (1999) 3324–3327.

[16] R.W. Mair, D. Hoffmann, S.A. Sheth, G.P. Wong, J.P. Butler, S. Patz, G.P. Topulos, R.L. Walsworth, Reduced xenon diffusion for quantitative lung study—the role of SF_6, NMR Biomed. 13 (2000) 229–233.

[17] J.B. West, Respiratory Physiology: The Essentials, Lippincott Williams & Wilkins, Baltimore, 2000.

[18] E.O. Stejskal, J.E. Tanner, Spin diffusion measurements: spin echoes in the presence of a time-dependent field gradient, J. Chem. Phys. 42 (1965) 288–292.

[19] P.T. Callaghan, Principles of Nuclear Magnetic Resonance Microscopy, Oxford University Press, New York, 1991.

[20] J. Stepisnik, Validity limits of Gaussian approximation in cumulant expansion for diffusion attenuation of spin echo, Physics B 270 (1999) 110–117.

[21] L.Z. Wang, A. Caprihan, E. Fukushima, The narrow-pulse criterion for pulsed-gradient spin-echo diffusion measurements, J. Magn. Reson. A 117 (1995) 209–219.

[22] B. Gross, R. Kosfeld, Anwendung der spin-echo-methode der messung der selbstdiffusion, Messtechnik 77 (1969) 171–177.

[23] M. Schachter, M.D. Does, A.W. Anderson, J.C. Gore, Measurements of restricted diffusion using an oscillating gradient spin-echo sequence, J. Magn. Reson. 147 (2000) 232–237.
[24] E.C. Parsons Jr., M.D. Does, J.C. Gore, Temporal diffusion spectroscopy: theory and implementation in restricted systems using oscillating gradients, Magn. Reson. Med. 55 (2006) 75–84.
[25] L.J. Zielinski, P.N. Sen, Effects of finite-width pulses in the pulsed-field gradient measurement of the diffusion coefficient in connected porous media, J. Magn. Reson. 165 (2003) 153–161.
[26] P.T. Callaghan, J. Stepisnik, Frequency-domain analysis of spin motion using modulated-gradient NMR, J. Magn. Reson. Series A 117 (1995) 118–122.
[27] J. Stepisnik, P.T. Callaghan, The long time tail of molecular velocity correlation in a confined fluid: observation by modulated gradient spin-echo NMR, Physica B 292 (2000) 292–301.
[28] A.L. Sukstanskii, D.A. Yablonskiy, Effects of restricted diffusion on MR signal formation, J. Magn. Reson. 157 (2002) 92–105.
[29] R.W. Mair, P.N. Sen, M.D. Hürlimann, S. Patz, D.G. Cory, R.L. Walsworth, The narrow pulse approximation and long length scale determination in xenon gas diffusion NMR studies of model porous media, J. Magn. Reson. 156 (2002) 202–212.
[30] M.D. Hurlimann, Effective gradients in porous media due to susceptibility differences, J. Magn. Reson. 131 (1998) 232–240.
[31] L.J. Zielinski, Effect of internal gradients in the nuclear magnetic resonance measurement of the surface-to-volume ratio, J. Chem. Phys. 121 (2004) 352–361.
[32] L.L. Latour, L. Li, C. Sotak, Improved PFG stimulated-echo methods for the measurement of diffusion in inhomogeneous fields, J. Magn. Reson. Series B 101 (1993) 72–77.